Adsorption-Mediated Mass Streaming in a Standing Acoustic Wave

Oren Weltsch, Avshalom Offner, Dan Liberzon, and Guy Z. Ramon*
Nancy and Stephen Grand Technion Energy Program and Department of Civil and Environmental Engineering, Technion—Israel Institute of Technology, Haifa 32000, Israel
(Received 1 December 2016; published 16 June 2017)

Oscillating flows can generate nonzero, time-averaged fluxes despite the velocity averaging zero over an oscillation cycle. Here, we report such a flux, a nonlinear resultant of the interaction between oscillating velocity and concentration fields. Specifically, we study a gas mixture sustaining a standing acoustic wave, where an adsorbent coats the solid boundary in contact with the gas mixture. It is found that the sound wave produces a significant, time-averaged preferential flux of a "reactive" component that undergoes a reversible sorption process. This effect is measured experimentally for an air-water vapor mixture. An approximate model is shown to be in good agreement with the experimental observations, and further reveals the interplay between the sound-wave characteristics and the properties of the gas-solid sorbate-sorbent pair. The preferential flux generated by this mechanism may have potential in separation processes.

DOI: 10.1103/PhysRevLett.118.244301

Oscillating flows, such as those that occur in acoustic fields, have the remarkable ability to generate nonzero time-averaged fluxes of heat and mass, despite the fact that the velocity field averages to zero over an oscillation cycle. Examples include second-order flows generated by fluctuating velocity components, where a broken symmetry results in nonzero higher-order time-averaged terms. Such symmetry breaking will occur if the amplitude or the phase of the oscillating velocity vary in space—typical of a standing and a travelling wave, respectively [1,2]. A time-averaged heat flux is generated in a standing acoustic wave through the interaction of oscillating velocity and temperature fields, and will generate cooling near pressure nodes (points of zero pressure amplitude) [3]. This effect can be used in refrigeration devices [4]. An acoustic mass flux may also be generated due to phasing between lateral motion and transverse thermal diffusion induced by temperature gradients [5–7].

Here, we describe the emergence of a significant, time-averaged mass flux within a gas mixture sustaining a standing acoustic wave. This particular "streaming" effect involves the pressure and velocity of the gas mixture, as well as the concentration of a "reactive" species that undergoes reversible sorption at a boundary. In this respect, it is an extension of the theoretically predicted flux based on evaporation or condensation [8] and shares some features with oscillatory Taylor-Aris dispersion with reactive boundaries [9–12]. However, while Taylor-Aris dispersion occurs *down the gradient*, the phenomenon described in this Letter *creates the gradient*. Further, this mechanism, unlike the thermal diffusion process described in [5–7], is driven by molecular diffusion and reversible sorption. We conceptualize the mechanism as follows: at any point within a quarter-wavelength resonator, a hydrodynamic "parcel" executes oscillatory motion accompanied by compression and expansion [see schematic in Figs. 1(b)–1(c)]. During the compression stage, which occurs in phase with the motion towards the pressure antinode (high-pressure side), the partial pressure of the reactive component increases and it will tend to sorb onto the boundary, driven by molecular diffusion; conversely, it will desorb as the pressure decreases during the motion towards the pressure node (low-pressure side). Over many such cycles (occurring at the frequency of the sound wave), a gradient in the composition is established, since the oscillating pressure amplitude varies spatially and so dictates the amplitude of compositional change during a cycle. This breaks the symmetry and creates a time-averaged flux, analogous to thermoacoustic streaming of heat [4].

In order to test the envisioned mechanism, we conducted experiments using air and water vapor as the gas mixture and zeolite-coated ceramics as the solid sorbent, placed in a quarter-wavelength resonator driven by a loudspeaker [see Fig. 1(a)]. Our results indicate that as soon as the sound field is created, water vapor is acoustically "pumped" towards the pressure antinode, and a humidity difference across the sorbent material is measured (see Fig. 2). To test the proposed physical mechanism, a theoretical model was formulated and validated against the experimental measurements, showing good agreement. The experimental system consisted of a 0.73-m-long, closed-ended polyvinyl chloride pipe with a 45.5-mm inner diameter, which served as the acoustic resonator. A sinusoidal, monochromatic signal of prescribed frequency and amplitude was generated in the resonator through a loudspeaker, driven by a personal computer-connected amplifier. The "heart" of the process is a porous material, the "stack," which serves as the source or sink of adsorbate during the acoustic exchange process. A commercially available 400-cells-per-square-inch, 2.5-cm-long ceramic honeycomb, washcoated with zeolite 13X adsorbent, was placed inside the resonator tube [see Fig. 1(a)].

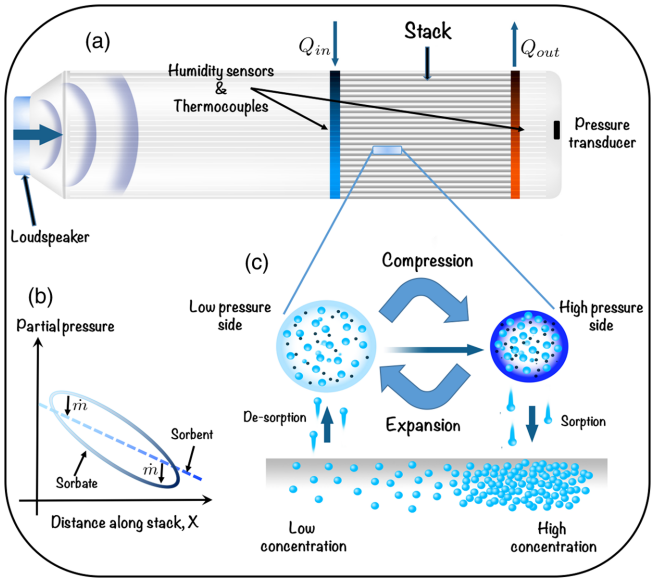

FIG. 1. (a) The experimental setup: a quarter-wavelength resonator in which a loudspeaker drives a standing wave at the resonant frequency and a controlled amplitude. The "stack" is coated with zeolite 13X adsorbent. Temperature is kept constant by heating and cooling at the stack edges, as indicated, measured by thermocouples. Humidity sensors at the stack edges measure the mass fraction of the water vapor. (b) The partial pressure of a representative gas "parcel" as it undergoes motion and compression; mass is exchanged in a direction dependent on the difference between the parcel's partial pressure and the local sorbent equilibrium. (c) Conceptual mass transfer mechanism combining motion, sorption, and diffusion. Gas expansion drives desorption, followed by motion towards the higher pressure, where compression drives sorption. The resulting time-averaged mass transfer creates accumulation close to the pressure antinode (high pressure) and depletion near the pressure node (low pressure).

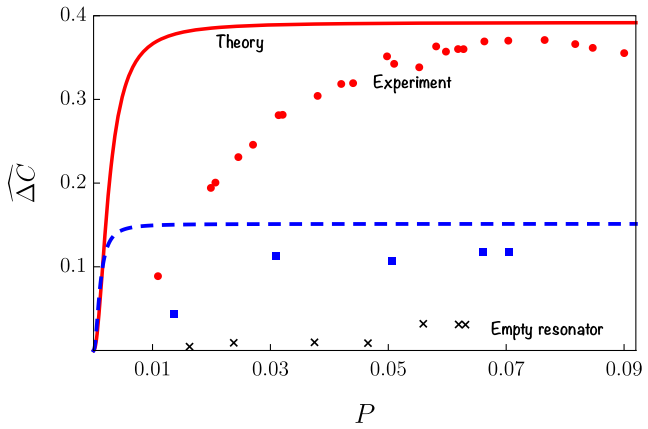

FIG. 2. The scaled concentration difference generated across the stack, $\widehat{\Delta C} \approx \Delta C/C_m$, as a function of the pressure amplitude, scaled against the mean pressure. The solid lines are model calculations, while dots represent experimental data. Results are shown for two stack positions, scaled against a quarter wavelength: 0.068 (red round markers) and 0.18 (blue square markers). Experimental measurements in the absence of the stack are presented as black crosses. Experimental conditions correspond with $\tau_\nu \approx 2.34$, $K \approx 20$.

In our experiments, the mixture used was humid air, in which water vapor was considered the reactive component that undergoes preferential sorption onto the zeolite-coated solid stack surface. The experimental goal was to measure the concentration difference across the stack, created by the streaming of water vapor. The experiments were kept under isothermal conditions, in order to isolate the mass-transfer effect from the coupled heat transfer; further, this eliminated the variations due to temperature, which affect the equilibrium conditions and, hence, the distribution of vapor. To maintain isothermal conditions, a spiral heating coil was placed at the stack side closest to the location of the pressure node, and its role was to compensate for the expected heat flux directed towards the pressure antinode. A heat sink was used to reject heat at the other side of the stack, while average temperatures, pressure fluctuations, and relative humidity were measured at various locations in the system [see the schematic in Fig. 1(a)]. More details of the experimental system, measurements, equipment used, and accuracy may be found in the Supplemental Material [13]. Preliminary measurements identified the fundamental resonant frequency of the system at $f \approx 105$ Hz; the longitudinal distribution of the pressure amplitude within the resonator followed a sinusoidal shape, with minimal distortion [14]. A typical experiment proceeded by driving an acoustic wave at the resonant frequency and a given amplitude while recording the temperature and humidity at either end of the stack. The heat input to the stack was adjusted so as to maintain a constant temperature throughout the experiment, until a steady concentration difference was established across the stack. This procedure was repeated to establish its reproducibility and then tested under systematic variations of pressure amplitudes ranging from 0.7 to 9.3 kPa. The time required to perform experiments covering the whole pressure range was ~12 hours, during which the relative humidity in the laboratory varied between 57% and 63%; however, the variations of relative humidity were found to be of little impact.

Experimental results showed an appreciable water vapor flux between the stack ends, detected through the mass fraction difference. Figure 2 shows the scaled concentration difference, $\widehat{\Delta C}/C_m$, measured at two stack locations, as a function of P, the pressure amplitude scaled against the ambient pressure, p_m; also shown are calculations from our model (presented below). In addition, results obtained in the absence of the stack (denoted as "empty resonator") are shown. When the stack is located further away from the pressure antinode, both measured and calculated values of $\widehat{\Delta C}$ are lower, generally showing the same trend of gradual increase and eventual saturation. Additional data obtained for the second resonant mode ($f \approx 310$ Hz, $\tau_\nu \approx 4$ [15]) showed an even sharper increase in concentration as the

pressure was increased, and achieved a degree of separation as good as that obtained for the lower frequency, at a lower pressure amplitude. This is a consequence of the higher transfer rate at increased frequency, and also the fact that the stack length (kept constant) becomes a larger fraction of the wavelength. At high pressure amplitudes, when the concentration gradient "saturates," the model and experiment are in rather good agreement. Meanwhile, at lower pressure amplitudes ($P \lesssim 0.5$) the theory deviates considerably from measurements. This can be explained by the low rates of mass-streaming near the pressure antinode, where the potential concentration difference increases but the rate at which mass is pumped decreases. This effect is enhanced at low pressure amplitudes. Since in our experiments the stack was placed relatively close to the pressure antinode, it is possible that at low pressure amplitudes the system had not reached a steady state. In addition, diffusion of material into the remainder volume of the resonator is not accounted for in our model and is another source of potential discrepancy.

In order to develop a better understanding of the underlying physics of the process, a model was formulated for a parallel-plate system contained within a resonator cavity filled with a binary gas mixture, in which a standing acoustic wave is sustained [see Fig. 1(a)]. The plates, separated by a distance $(2h)$, are much shorter than an acoustic wavelength and one component of the binary mixture undergoes reversible sorption onto the surface of the plates (coated with a thin layer of sorbent). All variables are decomposed into a mean and (small) fluctuating component, i.e., $g(x,y,t) = g_m(x) + \Re[g_1(y)e^{i\omega t}]$, where ω denotes the angular frequency of the oscillation and $\Re[\cdot]$ is the real part of a complex quantity. We are primarily interested in deriving the time-averaged, longitudinal mass flux of the reactive component,

$$\bar{\dot{m}} = \int_A \left(\overline{CNu} - \overline{ND\frac{\partial C}{\partial x}} \right) dA, \tag{1}$$

where A is the cross-sectional area, u and N are the axial velocity and molar density of the mixture, respectively, C and D denote the mole fraction and molecular diffusivity of the reactive component, respectively, and an overbar represents a time average over one period. In Eq. (1), the first term on the right is the mass-streaming term and the second term represents molecular diffusion. Expanding variables to second order in the fluctuations and performing the time averages [16], we find

$$\bar{\dot{m}} = \frac{1}{2} N_m \Re[\langle C_1 \tilde{u}_1 \rangle] - N_m D \frac{dC_m}{dx}, \tag{2}$$

in which $\langle\cdot\rangle$ denotes a cross-sectional average, the tilde denotes a complex conjugate, and the subscript 1 denotes a fluctuating quantity (see expansion above). This time-averaged mass flux, a second-order quantity commonly referred to as streaming, is expected to be larger than that which can be generated by the second-order bulk motion stemming from velocity fluctuations, e.g., Rayleigh streaming [1,2], or the acoustic mass flux generated by thermal diffusion effects [5–7].

In the limit $\omega L/a \ll 1$, where L is the plate (stack) length and a is the speed of sound, the advection-diffusion equation for the reactive species becomes [17]

$$i\omega C_1 + u_1 \frac{\partial C_m}{\partial x} = D \frac{\partial^2 C_1}{\partial y^2}. \tag{3}$$

Considering the sorption to be a first-order, reversible heterogenous reaction, we derive the following boundary condition, given here in nondimensional form [16]:

$$-\frac{N_m}{(1-C_m)\Lambda N^s} \frac{\partial C_1}{\partial Y}\bigg|_{Y=1} = \widehat{\mathrm{Da}}(C_m P_1 + C_{1|Y=1}), \tag{4}$$

in which N^s is the sorption capacity of the reactive component in the sorbent, $\Lambda = b/h$ is the ratio of adsorbent layer thickness to channel height, and

$$\widehat{\mathrm{Da}} = \frac{K\hat{\tau}_D^2}{1+\hat{\tau}_k^2} \tag{5}$$

is the complex Damköhler number, in which $K = k_a/k_d$ is the partition coefficient of the adsorbent, with k_a and k_d the sorption and desorption rate constants, respectively, $\hat{\tau}_k = (1+i)\tau_k$ where $\tau_k \equiv \sqrt{\omega/2k_d}$, and $\hat{\tau}_D^2 \equiv 2i(h/\delta_D)^2$ in which $\delta_D = \sqrt{2D/\omega}$ is the diffusive "penetration depth," the characteristic distance over which transverse diffusion occurs during half an oscillation cycle. The Damköhler number emerges in reaction-diffusion systems to signify the relative importance of each time scale; here, there is also the oscillation time scale and the phasing between diffusion and reaction. In case the sorbing layer is appreciably thick, it may be modeled as an additional domain in which diffusion and sorption occur [18].

Now, when $\widehat{\mathrm{Da}} \to 0$, for vanishingly slow kinetics, the boundary condition becomes that of a reflecting wall. If $\tau_k \gg 1$, i.e., in the limit of fast oscillations, the diffusion and reaction terms are in phase, while for fast kinetics, compared with the oscillations, $\tau_k \to 0$, they are out of phase. Further, when $\widehat{\mathrm{Da}} \gg 1$, kinetics dominate over both diffusion and the oscillation time scales, leading to the "ideal" relation $C_1 = -C_m P_1$, which illustrates that the boundary serves as a perfect source or sink of material, out of phase with the oscillating pressure. An increasing pressure drives material into the wall, reducing the concentration in the gas mixture; conversely, as the pressure becomes lower than the mean equilibrium pressure, material is driven out of the sorbent and the concentration in the gas increases. Furthermore, the magnitude of the

exchange is proportional to the mean fraction of the reactive component in the mixture. We also note that this limiting case represents, in a different notation, the boundary condition used by Raspet *et al.* [17].

Solving for the concentration field and performing the required integrations in Eq. (2) [16], we find the streaming, time-averaged mass flux,

$$\bar{\dot{m}} = N_m a \left\{ \frac{-C_m}{2(1+\mathrm{Sc})} \Re[P_1 \tilde{U}_1 \hat{F}] - \frac{\hat{G}|U_1|^2}{4\pi(1-\mathrm{Sc})} \frac{dC_m}{dX} - \frac{l}{2\pi} \frac{D}{La} \frac{dC_m}{dX} \right\}, \quad (6)$$

in which $\mathrm{Sc} = \nu/D$ is the Schmidt number, with ν the kinematic viscosity of the gas mixture, and $\hat{F}$ and $\hat{G}$ are complex functions of parameters representing the ratios of viscous, diffusive, and kinetic time scales, to the oscillation time scale [16]. The mass-streaming, as shown in Eq. (6), contains three terms; the first is the "acoustic" term, driven by the local pressure fluctuations that transfer mass from the solid to the gas and vice versa. This effect, combined with the spatial variation of the pressure amplitude, creates a longitudinal gradient in the time-averaged concentration. Once this gradient forms, it is countered by the two remaining terms: the hydrodynamic, modified Taylor-Aris dispersion, generated by oscillating flows in the presence of concentration gradients [11,12], and molecular diffusion.

In a closed resonator, as in our experiment, a concentration gradient will develop as mass is pumped acoustically along the stack from the low-pressure side (near the loudspeaker) to the high-pressure, closed end. At a given acoustic pressure amplitude, a corresponding concentration gradient will be reached as a steady state is established and $\bar{\dot{m}} \to 0$. Because of the presence of competing terms, we expect that the effect must be self-limiting, such that as one increases the acoustic forcing (the pressure amplitude), the sharper gradient created is dissipated to a greater extent by the dispersion term (which eventually dominates over the molecular diffusion term). Therefore, there will be a finite concentration gradient, which will remain constant even upon a further increase in pressure amplitude; we refer to this as the "limiting" concentration gradient, representing, in effect, the maximum achievable concentration difference. Using Eq. (6), setting $\bar{\dot{m}} = 0$, and assuming that the pressure and velocity distributions follow a standing wave, we numerically calculated the established gradient [16]. The following plots present the difference in the reactive component's molar fraction across the stack, scaled against the average mole fraction. This quantity, $\widehat{\Delta C}$, represents the ability to pump mass up the concentration gradient.

Figure 3(a) presents model calculations of $\widehat{\Delta C}$ as a function of $\tau_\nu (\equiv h\sqrt{\omega/2\nu})$, representing changes in resonance frequency, at different values of k_d (or, effectively, τ_k/τ_ν), denoting different desorption rates. The mass flux vanishes at $\tau_\nu \equiv h/\delta_\nu \to 0 (\tau_\nu \equiv h/\delta_\nu \to \infty)$, representing channel heights much smaller(larger) than the viscous penetration depth. A maximum is reached as $\tau_k/\tau_\nu \to 0$, or adsorption rates much faster than the oscillations. This maximum, characterized by $\tau_k/\tau_\nu \lesssim 10$ at high values of τ_ν, vanishes for $\tau_k/\tau_\nu \gtrsim 10$ leaving a plateau at low values of τ_ν. Any increase in τ_k narrows the frequency range of the mass pump and pushes it towards lower frequencies. In our experiments $\tau_\nu = 2.34$, which is an order of magnitude less than the optimum seen in Fig. 3(a) ($\tau_\nu \approx 22$). Accordingly, "tuning" the system resonance frequency with the stack geometry is a possible strategy for increased performance. Finally, Fig. 3(b) shows $\widehat{\Delta C}$ as a function of the equilibrium constant, K, for different values of τ_k; these parameters represent the properties of the sorbent-sorbate pair. All curves reach saturation ($\widehat{\Delta C} \approx 0.5$) for $K \to \infty$, representing ideal adsorption. The trend of the curves is determined by τ_k; very low values of τ_k, i.e., $\tau_k/\tau_\nu < 1$ (solid red line), represents fast kinetics where sorption occurs instantly. At higher values of τ_k, kinetics become comparable with the oscillation, reducing the system capacity to pump mass.

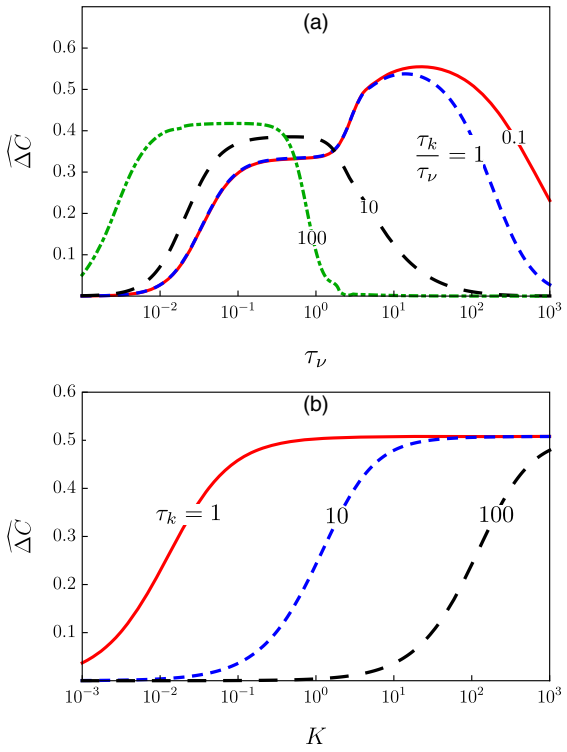

FIG. 3. The scaled concentration difference generated across the stack, $\widehat{\Delta C} \approx \Delta C/C_m$ as a function of (a) $\tau_\nu \equiv h\sqrt{\omega/2\nu}$ (here, $K = 20$) and (b) the partition coefficient, $K \equiv k_a/k_d$. In all calculations, $P = p_A/p_m = 0.06$.

In these preliminary experiments, our device has achieved a ~40% enrichment of the mixture, higher than the ~7% previously reported using acoustics [6]. A direct

comparison is unwarranted due to the use of different mixtures and acoustic fields; however, we point out that the separation achieved in our device occurs over a distance more than 10 times shorter than previously reported, illustrating that the gradient sustained by the mechanism proposed here can be substantially greater than is generated by thermal diffusion effects.

To summarize, we presented experimental measurements of a time-averaged mass flux generated preferentially for a single component in a gas mixture sustaining a standing acoustic wave. This flux is the result of the interaction between an oscillating velocity and a reversible sorption reaction with the boundary, driven by the pressure fluctuations. A theoretical model is shown to capture the experimental trends quite well and illustrates the importance of combining good affinity between the sorbing gas component and the sorbent solid, as well as fast kinetics and tuned frequency, in order to increase the capacity for pumping material. The mechanism explored in this Letter may pave the way for the development of devices for acoustic separation of gas mixtures.

O. W. and A. O. acknowledge the support from the Nancy and Stephen Grand Technion Energy Program (GTEP).

*ramong@technion.ac.il

[1] G. K. Batchelor, *An Introduction to Fluid Dynamics* (Cambridge University Press, Cambridge, 1967).
[2] N. Riley, Annu. Rev. Fluid Mech. **33**, 43 (2001).
[3] P. Merkli and H. Thomann, J. Fluid Mech. **70**, 161 (1975).
[4] G. W. Swift, J. Acoust. Soc. Am. **84**, 1145 (1988).
[5] G. W. Swift and P. S. Spoor, J. Acoust. Soc. Am. **106**, 1794 (1999).
[6] P. S. Spoor and G. W. Swift, Phys. Rev. Lett. **85**, 1646 (2000).
[7] D. A. Geller and G. W. Swift, J. Acoust. Soc. Am. **112**, 504 (2002).
[8] W. V. Slaton, R. Raspet, C. J. Hickey, and R. A. Hiller, J. Acoust. Soc. Am. **112**, 1423 (2002).
[9] M. Shapiro and H. Brenner, Chem. Eng. Sci. **41**, 1417 (1986).
[10] B. S. Mazumder and S. K. Das, J. Fluid Mech. **239**, 523 (1992).
[11] C. O. Ng, Int. J. Eng. Sci. **38**, 1639 (2000).
[12] G. Ramon, Y. Agnon, and C. Dosoretz, Microfluid. Nanofluid. **10**, 97 (2011).
[13] See Supplemental Material at http://link.aps.org/supplemental/10.1103/PhysRevLett.118.244301 for additional details of the experimental setup and procedure.
[14] See Supplemental Material at http://link.aps.org/supplemental/10.1103/PhysRevLett.118.244301 for measurements of the longitudinal variation of the pressure amplitude.
[15] See Supplemental Material at http://link.aps.org/supplemental/10.1103/PhysRevLett.118.244301 for measurements of the concentration difference at higher frequency.
[16] See Supplemental Material at http://link.aps.org/supplemental/10.1103/PhysRevLett.118.244301 for derivation.
[17] R. Raspet, W. Slaton, C. Hickey, and R. Hiller, J. Acoust. Soc. Am. **112**, 1414 (2002).
[18] M. Nori and S. Brandani, J. Acoust. Soc. Am. **135**, 2634 (2014).